Physical Mechanisms Limiting the Manufacturing Yield of Millimeter-Wave Power InP HEMTs

S. Krupenin, R. R. Blanchard, M. H. Somerville, J. A. del Alamo, K. G. Duh* and P. C. Chao*

Massachusetts Institute of Technology, Rm. 39-427, Cambridge, MA 02139, USA;

* Sanders Lockheed Martin, Nashua, NH 03061, USA

ABSTRACT

We have developed a methodology to diagnose the physical mechanisms limiting the manufacturing yield of millimeter-wave power InAlAs/InGaAs HEMTs on InP. A statistical analysis was carried out on DC figures of merit obtained from a large number of actual devices on an experimental wafer. Correlation studies and a Principal Component Analysis (PCA) of the results indicated that variations in Si delta-doping concentration introduced during MBE accounted for more than half of the manufacturing variance. Variations in the gate-source distance that is determined by the electron-beam alignment in the gate formation process were the second leading source of manufacturing variance.

INTRODUCTION

The InP HEMT is the leading contender for high-power high-efficiency millimeter-wave power amplifiers (Smith (1)). As the InP HEMT technology matures, manufacturing issues come to the foreground. To date there has been little work on understanding the key factors affecting the manufacturing yield of these devices. Such a study is been hampered by the considerable amount of work that it takes to measure millimeter-wave power figures of merit. Manufacturing yield improvement is critical because high cost represents a significant road block in the development of millimeter-wave systems.

In this work we have carried out a statistical study of DC figures of merit of InP power HEMTs that strongly impact the millimeter-wave performance of these devices. All of the selected figures of merit were measured in actual devices. A statistical analysis of the results using the PCA revealed the physical sources of variability in these figures of merit. Our methodology can be easily implemented in a manufacturing environment for continuous process diagnostics and improvement.

EXPERIMENTAL

The devices studied in this work are 0.1 um gate length and 25 um gate width double-heterostructure InP power HEMTs on an experimental 3-inch wafer from Lockheed Martin Sanders (Putnam et al (2) and Somerville et al (3)). The devices feature a selectively recessed depleted cap. A total of 50 devices located on every other die of the wafer were studied. All figures of merit were measured with the same probe configuration, allowing fast and completely automated measurements.

Ten DC figures of merit were selected to capture the key millimeter-wave power figures of merit. They are listed in Table 1. Threshold voltage, V_T, is of ubiquitous importance in device operation. Maximum transconductance, GM_{max}, is closely related to f_T and also determines the millimeter-wave gain of the transistor. The gate-source voltage at which GM_{max} occurs, VGS_{gmmax}, has to be well controlled for optimal biasing of the transistor. The power output of the transistor is determined by the maximum drain current ID_{max} as well as the off- and on-state breakdown voltages, BV_{dg_off}, BV_{ds_off} and BV_{ds_on}. Output conductance, G_d, should be as small as possible for maximum gain. Extrinsic source and drain resistances, R_s, and R_d, are important parasitics that affect power efficiency and the gain of the transistor in many amplifier configurations. The measurement conditions for these figures of merit are also summarized in Table 1. This table also lists the mean and standard deviation of each figure of merit.

The correlation matrix of the figures of merit is shown on Fig. 1. Each vignette lists the correlation coefficient between the two figures of merit. Some of the correlation coefficients on Fig. 1 can be interpreted directly. For example, R_s and R_d exhibit a strong positive correlation coefficient of 0.68, which suggests a contact resistance or doping level problem and excludes misalignment of the gate process from being a dominant source of variation in these figures of merit. In general, however, just from examination

of the data in Fig. 1 it is not possible to uncover the physical sources of variability. In order to further our insight into the physics underlying variations in the figures of merit we have performed a Principal Component Analysis (PCA) of the data.

PRINCIPAL COMPONENT ANALYSIS

PCA performs a coordinate transformation from the original space of electrical measurements to a new space of uncorrelated "principal components". These are ordered according to the total variance that they account for in the original data: first the variance explained by P1 is maximized; then the second component, P2, is selected to maximize the variance of the residual after P1 is removed, and so on. A comprehensive treatment of PCA can be found in Morrison (4). In a first pass, all figures of merit were weighted equally. Customer demands can be taken into account by introducing appropriate weights.

The relative contribution of each principal component to the variance is shown in Fig. 2. This figure shows that the most significant component, P1, accounts for 51% of the total variance of the process. Correct identification of this component followed by appropriate corrective action can significantly improve the manufacturing yield. The second and the third components account for 21% and 13% of the total variance respectively. The rest of the components add up to a total of 15%. In order to carry out the identification of the principal components, their relative impact on each DC figure of merit should be examined. Fig. 3 shows a percentage of the variance of each figure of merit that is attributed to each principal component. For example, P1 accounts for nearly 80% of the variance of V_T. These percentages are statistically significant for each of the three most important components. The standard deviations of the weights of the first three principal components towards any figure of merit did not exceed 9% under the assumption of a multivariate normal distribution (Morrison (4)). Hence Fig. 3 is a reliable vehicle for physical identification of the principal components.

Spatial distributions of the principal components can also be constructed. They are exhibited on Fig. 4. The circular symmetry of P1 and the linear gradient distributions of P2 and P3 offer further clues for identification of these quantities.

Close study of the results on Fig. 3 allowed us to conclude that the only interpretation of P1 that is consistent with the weights and the signs of the correlations between P1 and the various figures of merit that it affects is that P1 is related to the sheet electron concentration in the channel, n_s. P1 accounts for 78% of the variance in V_T, and the correlation is negative, which is consistent with the fact that higher n_s increases the inversion charge in the channel that has to be depleted by applying a negative gate-source bias. The impact of P1 on ID_{max} is also large (77%) and positive: n_s is proportional to the number of carriers in the channel. P1 further has a relatively large negative impact on variances of all three breakdown voltages. The negative correlation of n_s and BV_{ds_on} is a result of the positive dependence of n_s on the impact ionization coefficient (Somerville (3)). Negative dependence of BV_{dg_off} and BV_{ds_off} on n_s is predicted by a tunneling-limited off-state breakdown model proposed by Somerville and del Álamo (5). Since n_s is the dominant factor in the channel conductivity, the negative correlation of P1 and the parasitic resistances R_s and R_d is also consistent with this interpretation of P1. The positive correlation of P1 with GM_{max} and G_d follows from that with ID_{max}. The relatively weak correlation of P1 with GM_{max} enables us to further narrow down P1 to the concentration of Si dopants in the delta-doping layers as opposed to other sources of variability in n_s such as the insulator thickness. Finally, higher n_s leads to a more negative V_T, which shifts the whole g_m vs. V_{gs} curve to the left, decreasing VGS_{gmmax}. The circular symmetry of the spatial distribution of P1 over the wafer, shown on Fig. 4, is consistent with this interpretation of P1 since Si dopants are introduced in the MBE process while the wafer is rotating in front of the Si gun.

P2 is seen in Fig. 3 to correlate negatively with GM_{max} and VGS_{gmmax} and positively with R_s, but not V_T. This indicates that P2 is likely to be related to gate-source distance variations, probably determined by the reproducibility of the positioning of the electron beam used to write the gate. P2 has a roughly linear distribution on the wafer as one would expect from a process of this kind. P3 only affects G_d, BV_{dg_off}, and R_d, which suggests a strong association with the extrinsic drain portion of the device. Its detailed origin still remains unknown to us. Fig. 5 shows a schematic diagram of the device indicating the physical interpretation of P1 and P2.

Measurements on Transmission Line Model (TLM) test structures were used as an independent verification of the identification of P1 as the Si delta-doping concentration and its direct impact on the sheet carrier concentration n_s. The saturation current in a TLM structure obtained when a relatively high voltage is applied is directly proportional to n_s and v_{sat}. The saturation current was measured in 100 um wide and 50 um long TLM structures at 10 V. We have found a very close correlation across the wafer between P1 and the TLM saturation current measured on a test structure on the same die (Fig. 6): the correlation coefficient is 0.84. This gives us confidence that the identification of P1 is correct.

Our findings are in substantial agreement with those of Elliott et al (6) on TRW's 3-inch fabrication line for InP-based HEMT and HBT MMIC's. These authors single out MBE growth as the most critical node in InP HEMT MMIC production in agreement with the MBE origin of P1 in our work. Additionally, they identified gate formation as the second most critical node for HEMTs. They found that gate length and gate-source spacing are critical parameters. While we have not been able to isolate the impact of the gate length variations, we relate P2 to the distance between the gate and the source, in agreement with the findings in (6).

CONCLUSIONS

In summary, we used a Principal Component Analysis to identify the two most important sources of manufacturing variability in InP power HEMTs: the concentration of Si dopants in the delta-doping layers of the device and the distance between the gate and the source. Jointly these two components account for 72% of manufacturing variations. Our findings are in agreement with those reported by Elliott et al (6) on TRW's InP based MMIC fabrication line. Necessary statistical data was obtained from simple DC measurements on actual transistors – no specialized test structures were required. Our methodology can be easily implemented in a manufacturing environment for continuous process yield diagnostics and improvement.

ACKNOWLEDGEMENT

This research was funded by the MAFET program, through Sanders Lockheed Martin.

REFERENCES

(1) P.M. Smith, "InP-HEMTs for Microwave and Millimeter-wave Applications," 1995, International Conference on InP and Related Materials, pp. 68-72.

(2) C.S. Putnam, M.H. Somerville, J.A. del Alamo, P.C. Chao, and K.G. Duh, "Temperature Dependence of Breakdown Voltage in InAlAs/InGaAs HEMTs: Theory and Experiments," 1997, International Conference on InP and Related Materials, pp. 197-200.

(3) M.H. Somerville, R.R. Blanchard, J.A. del Alamo, P.C. Chao, and K.G. Duh, "On-State Breakdown in Power HEMTs: Measurements and Modeling," 1997, International Electron Devices Meeting, pp. 553-556.

(4) D.F. Morrison, "Multivariate Statistical Methods," 1990, McGraw-Hill, pp. 313-317.

(5) M.H. Somerville and J.A. del Alamo, "A Model for Tunneling-Limited Breakdown in High-Power HEMTs," 1996, International Electron Devices Meeting, pp. 35-38.

(6) J. Elliott, L. Tran, R. Lai, T. Block, J. Cowles, D. Tran, W. Jones, Y.C. Chen, A. Oki and D. Streit, "A Flexible 3-Inch Fabrication Line for InP-Based HEMT and HBT MMIC Production," 1997, International Conference on InP and Related Materials, pp. 501-504.

Symbol	Variable	Measurement Conditions	Mean	St. dev.	Units
V_T	Threshold voltage	V_{ds}=1.2 V, I_D=1 mA/mm	-1.442	0.072	V
GM_{max}	Maximum transconductance	V_{ds}=1.2 V	718	49	mS/mm
VGS_{gmmax}	Gate-source bias at which GM_{max} occurs	V_{ds}=1.2 V	-0.656	0.078	V
ID_{max}	Maximum drain current	V_{ds}=1.2 V, V_{gs}=0.4 V	846	68	mA/mm
G_d	Output conductance	V_{ds}=1.2 V, V_{gs}=0 V	91	11	mS/mm
BV_{dg_off}	Drain-gate off-state breakdown voltage	I_D = 1 mA/mm, I_G =-1 mA/mm	3.85	0.21	V
BV_{ds_off}	Drain-source off-state breakdown voltage	I_D = 1 mA/mm, I_G =-1 mA/mm	2.09	0.26	V
BV_{ds_on}	Drain-source on-state breakdown voltage	I_D = 200 mA/mm, I_G =-1 mA/mm	1.63	0.14	V
R_s	Source resistance	I_S=I_G=100 mA/mm, I_D=0	9.60	1.5	Ω
R_d	Drain resistance	I_D=I_G=100 mA/mm, I_S=0	12.2	2.0	Ω

Table 1: Definitions and the measured values of the DC figures of merit (L_g = 0.1 um, W_g = 25 um).

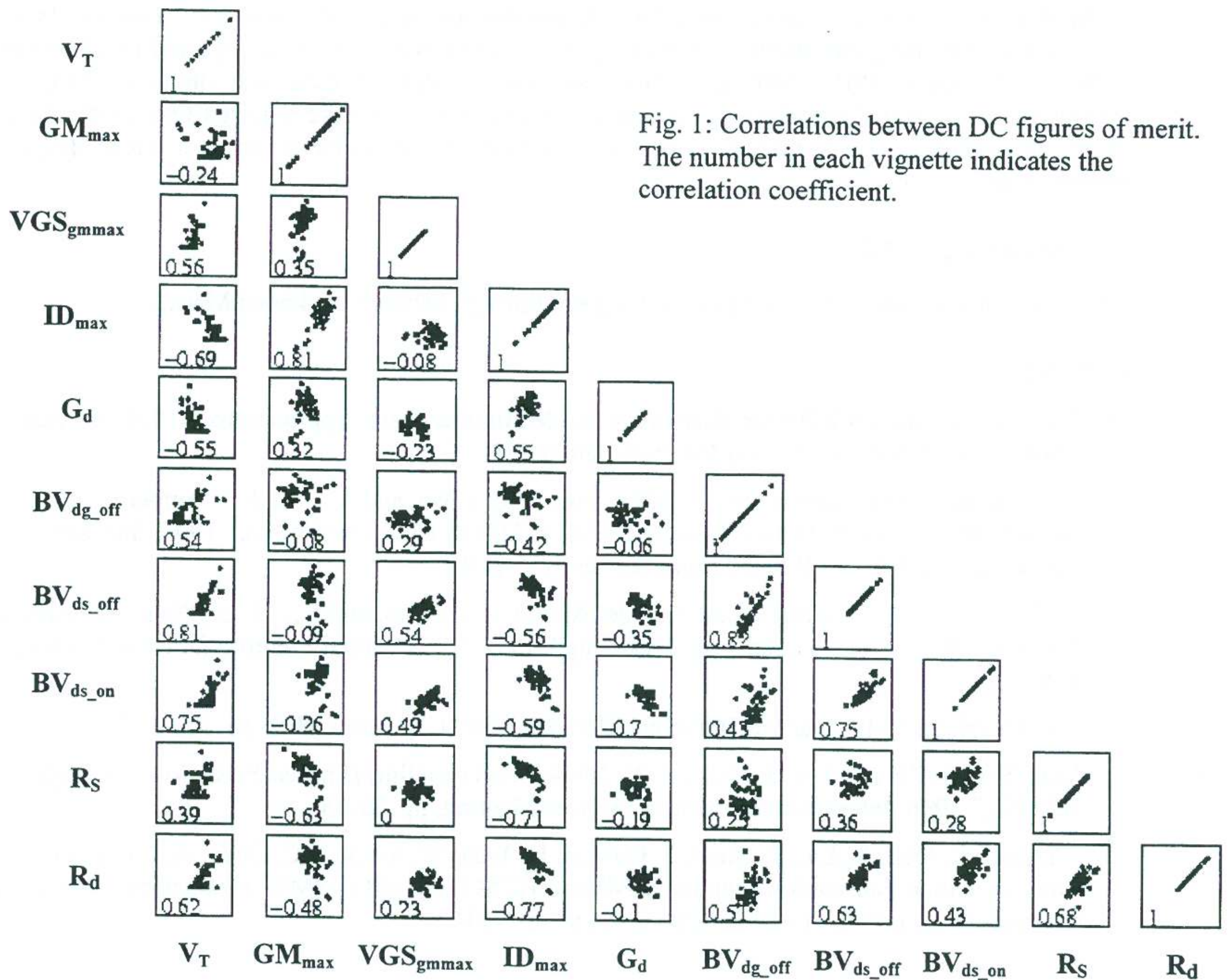

Fig. 1: Correlations between DC figures of merit. The number in each vignette indicates the correlation coefficient.

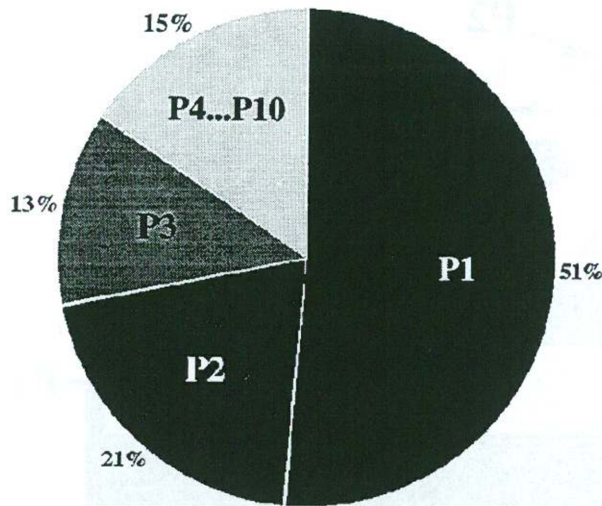

Fig. 2: Relative importance of the principal components in the manufacturing variance. P1 explains 51% of the variance of the manufacturing process.

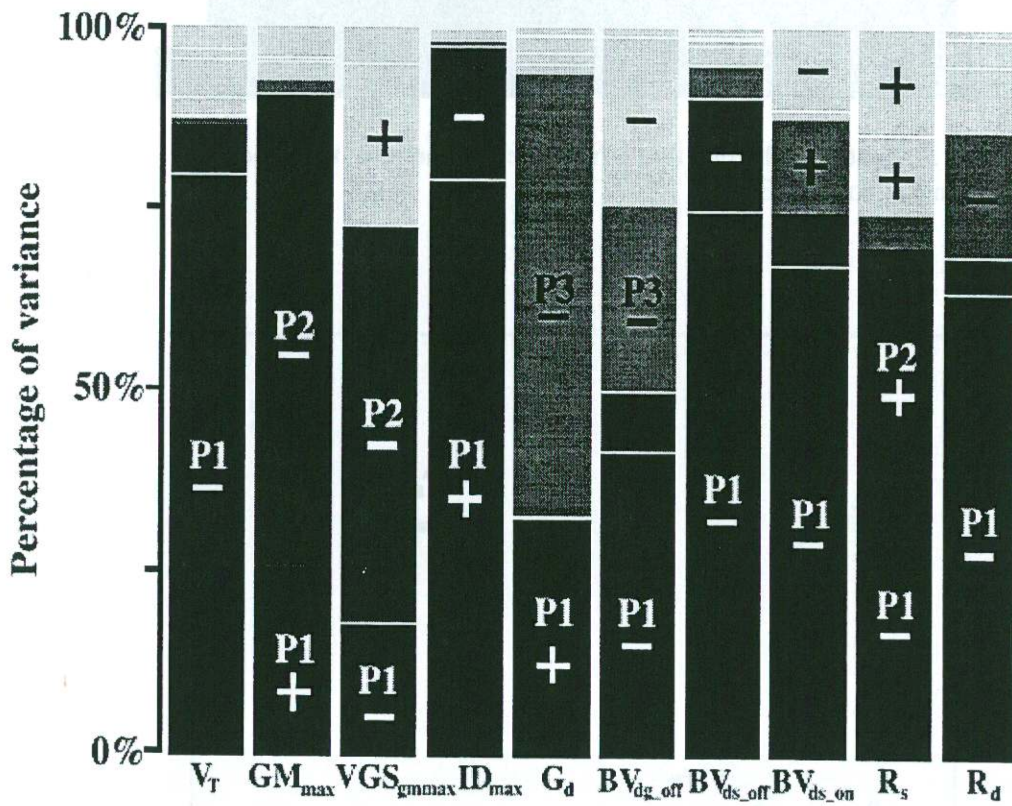

Fig.3: Contributions of each of the principal components to the variance of each DC figure of merit. The signs indicate whether a component has a positive or negative correlation with a given figure of merit.

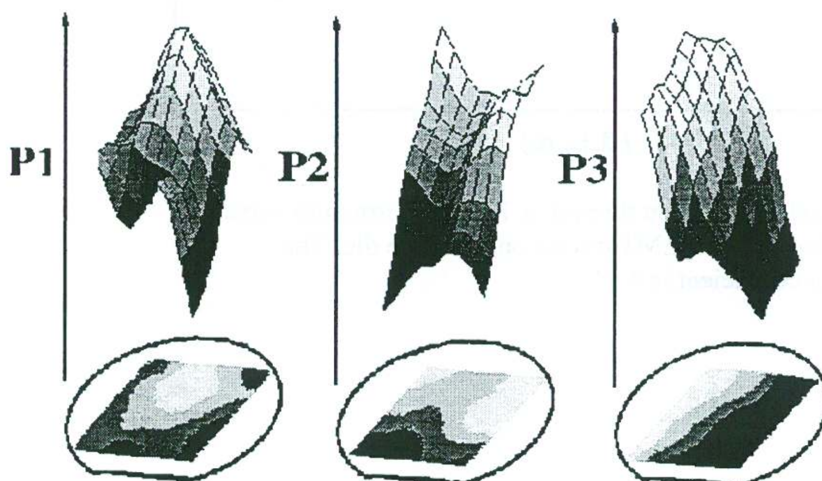

Fig. 4: Spatial distributions on the wafer of the first three principal components. Notice that the first component, P1, has a radial distribution, while P2 and P3 exhibit linear gradients.

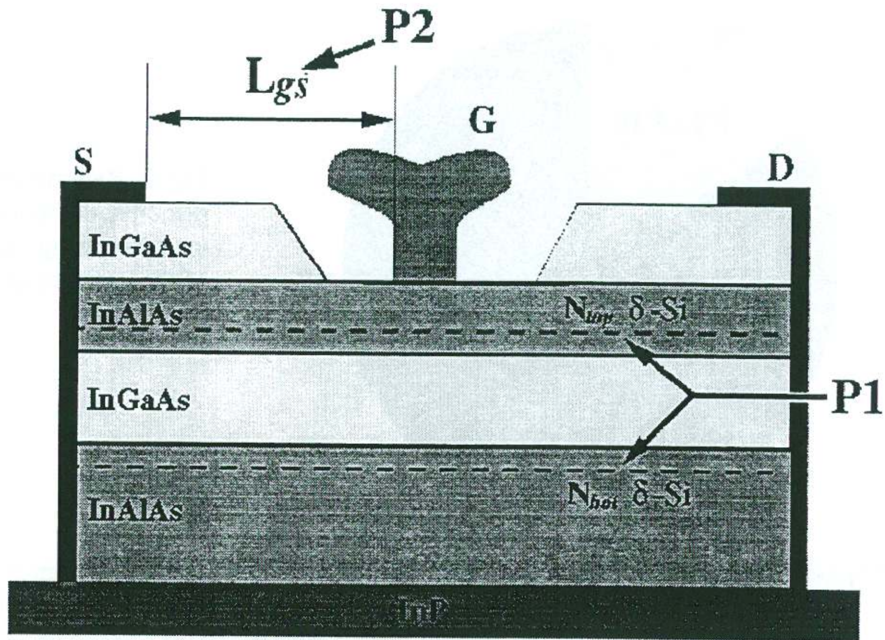

Fig. 5: Identity of the first two principal components in the structure of an InP power HEMT.

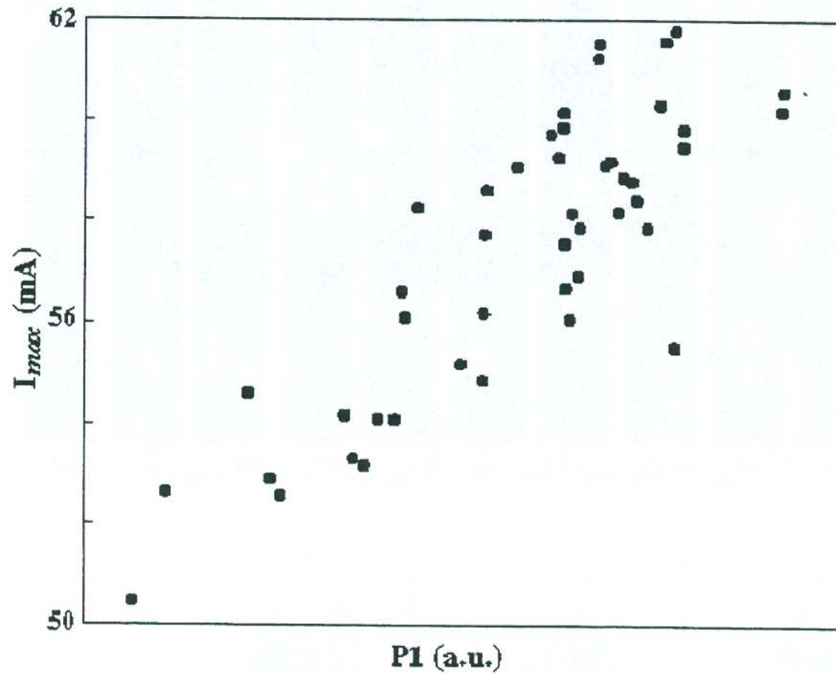

Fig. 6: Maximum current through a TLM test structure versus the P1 value for the HEMT device on the same die. The correlation coefficient is 0.84.